

PACS numbers: 87.50.W – ; 87.50.wp; 36.40.Gk; 78.67.Bf
DOI: 10.1070/QE2008v038n06ABEH013863

Laser photothermolysis of biological tissues by using plasmon-resonance particles

I.L. Maksimova, G.G. Akchurin, G.S. Terentyuk, B.N. Khlebtsov, G.G. Akchurin Jr., I.A. Ermolaev, A.A. Skaptsov, E.M. Revzina, V.V. Tuchin, N.G. Khlebtsov

***Abstract*. The spatial temperature distribution in biological tissues upon interaction of laser radiation with plasmon-resonance nanoparticles is simulated numerically. Experimental thermograms of model objects and real biological tissues are obtained *in vivo* for different localisation depths of nanoparticles in different irradiation regimes. The results obtained in the study can be used for the development of methods of laser photothermolysis of malignant tumours.**

Keywords: *photothermolysis, plasmon resonance, biological tissue, nanoparticles.*

1. Introduction

The unique optical properties of plasmon-resonance nanoparticles along with a high specificity of biomolecular recognition open up new possibilities for their applications in biomedical diagnostics [1], directed drug delivery [2], and optical visualisation and photothermal therapy [3, 4]. The possibilities of optimisation of nanoparticle parameters and laser irradiation regimes during photothermal action in oncology were considered in papers [5, 6].

The application of plasmon-resonance nanoparticle in biomedicine has two main aspects: biospecific 'aiming' at certain tissues or cells and optical plasmon resonance [1 – 5]. The addressed accumulation of particles inside a biological target or near it can be achieved passively or actively. In the first case, non-functionalised inert particles are accumulated inside a specified biological target due to size-determined effects. For example, nanoparticles with a silicon nucleus and a gold shell with external diameter 130 nm penetrate through vessel walls and are accumulated in malignant tumour tissues having a high vascularization due to neoangiogenesis and the enhanced porosity of vessel walls [7]. The second, active approach is based on the use of particle conjugates with biospecific molecules, for example, tumour-specific antibodies, which can provide their specific delivery to malignant cells. Such a procedure of conjugate formation is called functionalisation [8], and the term 'conjugate' is often used to refer to functionalised nanoparticles [9, 10]. An optical plasmon resonance is caused by coherent oscillations of free electrons in metals under the action of the electric component of a light wave. These oscillations enhance the scattering and absorption of light at resonance wavelengths caused by the multipolarity of the polarisability tensor. By exposing nanoparticles to laser radiation at a wavelength in the region of their absorption band, it is possible to produce the local heating of nanoparticles and surrounding cells or the localised extraction of an incapsulate drug. The first method forms the basis of photothermal therapy [4], while the second one is related to the address delivery of drugs [2, 11].

To perform efficiently photothermal therapy of malignant tumours, it is necessary to match three important factors: the laser radiation wavelength, the absorption maximum of light by gold nanostructures, which are used as selective absorbers, and the transparency of a tissue for laser pulses. It is known that the optical transparency window of biological tissues covers the near-IR spectral range from 750 to 1100 nm. The lower boundary of the range is determined by strong scattering of short-wavelength radiation in biological tissues and absorption of light by melanin and blood, while the upper limit is determined by absorption of light in water. The spectral shift of plasmon resonances to the near-IR range is a principal factor for photothermal therapy and can be achieved only by using structured nanoparticles or nanorods [12, 13] because usual gold nanospheres have a broad resonance only in the visible region.

The use of gold nanorods and nanoshells makes it possible to tune a plasmon resonance in a broad spectral range (from 600 to 1500 nm) by varying the axial coefficient of nanorods or relation between the nucleus diameter (SiO_2) and the gold shell thickness (Au). We used in our experiments plasmon-resonance gold nanoshells fabricated at the laboratory of biosensors and nanostructures at the Institute of Biochemistry and Physiology of Plants and Microorganisms, RAS (Saratov).

I.L. Maksimova, G.G. Akchurin, G.S. Terentyuk, G.G. Akchurin Jr., I.A. Ermolaev, A.A. Skaptsov, E.M. Revzina, V.V. Tuchin
N.G. Chernyshevsky Saratov State University, ul. Astrakhanskaya 83, 410012 Saratov, Russia; e-mail: irina_mksmv@yahoo.com, AkchurinGG@mail.ru, vetklinika@front.ru, irmolaev@rambler.ru, Skaptsov@yandex.ru, lesya16@bk.ru, tuchin@sgu.ru;
B.N. Khlebtsov, N.G. Khlebtsov N.G. Chernyshevsky Saratov State University, ul. Astrakhanskaya 83, 410012 Saratov, Russia; Institute of Biochemistry and Physiology of Plants and Microorganisms, Russian Academy of Sciences, prosp. Entuziastov 13, 410049 Saratov, Russia; e-mail: khlebtsov@ibppm.sgu.ru

Received 7 March 2008; revision received 25 April 2008
Kvantovaya Elektronika **38** (6) 536 – 542 (2008)
Translated by M.N. Sapozhnikov

2. Theoretical simulations

2.1 Spatial distribution of absorbed laser radiation

We simulated the spatial distribution of absorbed photons during the propagation of an electromagnetic wave through a system of discrete particles taking multiple scattering into account. The diffusion scattering of laser radiation at 808 nm in a disperse system of gold nanoparticles was calculated by the Monte-Carlo method. Simulations were performed for gold spherical nanoshells with a SiO_2 nucleus. The nucleus diameter was 140 nm and the gold shell thickness was 15 nm. The extinction maximum of these particles is located at $\lambda \sim 800$ nm. The trajectories of 10^7 photons were calculated in simulations. A chain of random events consisting in the displacement of a photon by some distances, scattering or absorption by a particle was simulated for each photon with the help of a random number generator. The scattering probability in the specified direction in each scattering event was determined for a particle with the specified diameter of a silicon nucleus and the gold shell thickness by using the Mie theory. The realisation of scattering or absorption in each interaction event between a photon and a particle is also a random process, whose probability is determined by the relation between the extinction and scattering coefficients. The values of the real and imaginary parts of the refraction index of gold taking into account dispersion in the spectral range of interest to us were borrowed for experimental papers [14–16].

We used in calculations the polarisation-averaged angular dependence of the scattering intensity by neglecting polarisation effects. According to [17], such averaging in the case of a nonpolarised incident beam and multiple scattering leads to the error that does not exceed a few percent.

Figure 1 shows the spatial distribution of the absorbed radiation power at the plasmon-resonance frequency for gold nanoshells with a SiO_2 nucleus uniformly distributed in water. It was assumed in simulations that incident radiation propagated perpendicular to the surface of an infinite horizontal layer containing nanoparticles (shown by the arrow in the figure). Variations in the concentration of particles and, correspondingly, in the scattering regime (from single to multiple scattering) lead to changes in the spatial distribution of the absorbed power. If the concentration of particles is high, laser radiation is predominantly absorbed near a surface, while at low concentrations the radiation can penetrate much deeper. The grey scale in Fig. 1 corresponds to different densities of photons absorbed at a given point.

The model of a medium infinite in the transverse direction can be used in calculations of the spatial distribution of absorbed photons because the laser beam diameter (2 mm) is small compared to the diameter (10 mm) of the cell containing the suspension of particles. Our calculations show that the fraction of photons reaching the cell walls does not exceed hundredths of percent and the neglect of boundary effects in this case does not affect the final result.

In real applications of hyperthermia, tumours are often located not on the tissue surface but at some depth [18]. Therefore, if the selective accumulation of particles in a tumour tissue was achieved, their concentration will be also maximal at some distance from the surface. The problem is to perform the hyperthermia of such a tumour without damaging upper-lying tissues [19]. The model calculations of the spatial distribution of absorbed photons presented below allow us to estimate the maximum depth of the region of the enhanced concentration of particles at which the level of absorbed energy is sufficient for increasing temperature in this region by the specified value. A biological tissue was simulated in calculations by a system of weakly absorbing spherical particles with the refractive index $1.44 + i0.0001$, which were embedded into a medium with the refractive index 1.34. One of the methods for increasing the volume density of absorbed laser energy in the required region is the laser beam focusing. Computer modelling should help us to estimate the efficiency of such focusing in real biological tissues, when the laser beam is broadened due to scattering. We considered in simulations the cases of a parallel incident beam and a beam focused at the centre of a layer or a spherical volume with nanoparticles.

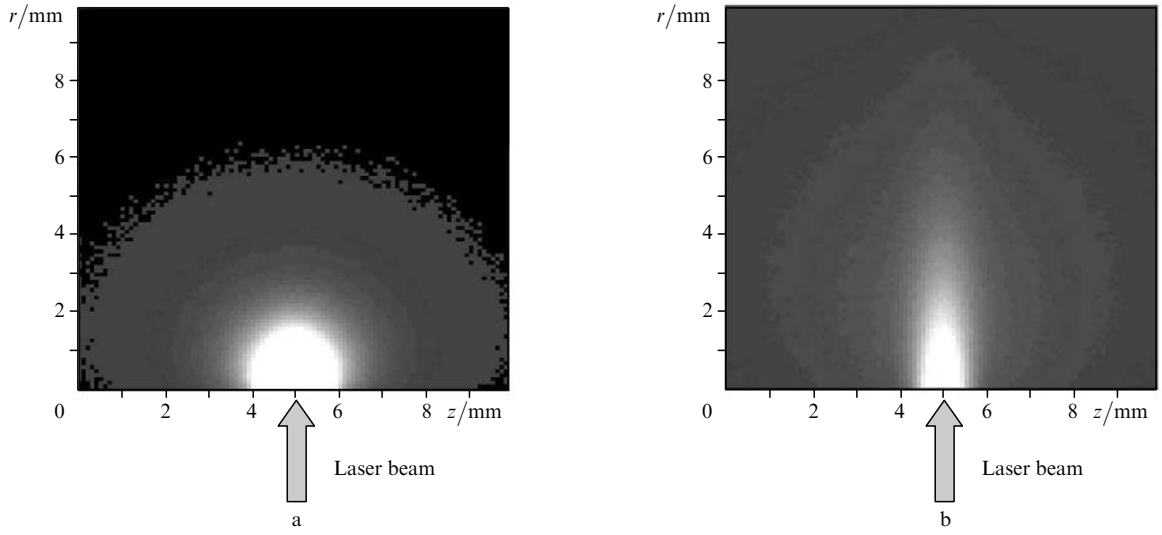

Figure 1. Computer simulations of the spatial intensity distribution of absorbed laser radiation in the suspensions of nanoparticles at concentrations 5×10^9 (a) and 1×10^9 mL^{-1} (b).

It is also interesting to consider situations when the laser beam diameter is comparable with the diameter of the region of high concentration of nanoparticles or larger. The region containing nanoparticles was assumed spherical in calculations. Figure 2 shows that upon irradiation by a broad parallel beam, a greater part of photons are absorbed in the front half of the region (region II), whereas upon focusing the beam to the centre of the region, absorbed photons are localised near the beam waist and on the front surface of this spherical region. The grey scale (at the right) corresponds to the density of absorbed photons on a surface 10 μm^2 in the range 0–0.01 % of the total number of incident photons.

2.2 Calculation of temperature fields

Calculations of temperature effects appearing due to absorption of laser energy by nanoparticles should take into account the finite volume of the suspension of gold particles and heat transfer at the cell walls because due to the thermal diffusion the region of elevated temperatures greatly exceeds the region in which a greater part of absorbed photons is localised.

The axial symmetry of the calculation region allows us to simulate thermal processes by using the two-dimensional Poisson equation written in the cylindrical coordinate system [20]:

$$\mathrm{div}[\lambda \,\mathrm{grad}\, T(r,z)] = Q(r,z),$$

where λ is the heat-transfer coefficient; r and z are the transverse and longitudinal coordinates; $T(r,z)$ is the temperature distribution; $Q(r,z)$ is the internal heat release power caused by the absorbed laser radiation. The thermal properties of water and cell walls were assumed constant, and the symmetry axis of the calculation region coincided with the laser beam axis.

Heat exchange at boundaries was modelled by the boundary conditions

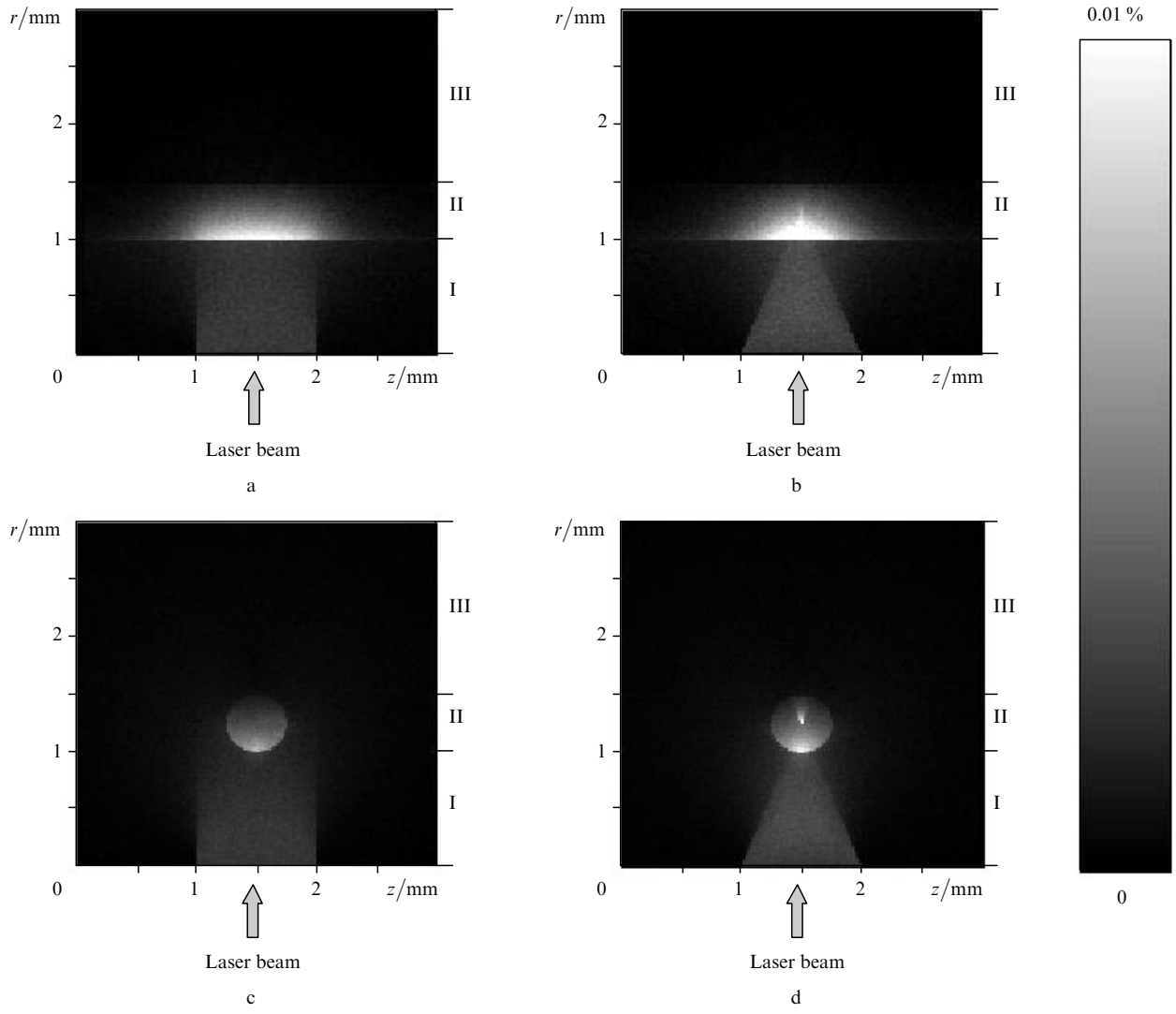

Figure 2. Computer simulations of the spatial distribution of laser power absorbed in structured systems containing nanoparticles: (a, b) layered structure: 1-mm-thick layer I contains weakly absorbing scattering particles (the volume fraction of particles of diameter 0.5 μm is 0.1); 0.5-mm-thick layer II contains, along with weakly absorbing particles, 15-nm-thick gold nanoshells with a silicon nucleus of diameter 140 nm; layer III, as layer I, contains weakly absorbing scattering particles; (c, d) in a medium with scattering particles, a sphere of diameter 0.5 mm is located, which contains, along with scattering particles, plasmon-resonance gold nanoshells with the same parameters as in Figs 2a, b.

$$\lambda\frac{\partial T}{\partial r}\bigg|_{r=R} = \alpha_1(T|_{r=R} - T_0), \quad \lambda\frac{\partial T}{\partial z}\bigg|_{z=0} = \alpha_2(T|_{z=0} - T_0),$$

where α_1 and α_2 are the heat-transfer coefficients on the side and open boundaries of the region and T_0 is the temperature of the environment, which was set equal to 25 °C in simulations.

The Poisson equation was solved by the Galerkin method of finite elements (weak formulation). Temperature was approximated by a linear combination of basis functions (shape functions) on linear triangular finite elements. A system of algebraic equations was solved by the Gauss method for banded matrices. Calculations were performed on a nonuniform finite-element network with a total number of nodes equal to 1800.

We calculated the isotherms of stationary temperature fields for thermal sources $Q(r, z)$ obtained by computer simulations for particles at concentrations 5×10^9 and 1×10^9 mL^{-1}, which were contained inside cylindrical volumes of the same dimensions as those of 'eppendorf' cells used in experiments (the cell diameter and height were 10 and 40 mm, respectively). In the case of high concentrations of particles, the temperature maximum is located near the liquid surface and is 63.4 °C. Near the side walls and at the top of the cell, temperature decreases down to 62.2 °C due to heat transfer from the liquid surface and through side walls. The maximum temperature drop in the scattering volume under study is $T_{max} - T_{min} = 24.5$ °C. In the second case, when the concentration of particles is 10^9 mL^{-1}, the total heating is weaker, however, the temperature maximum equal to 45.4 °C is located at a distance of 4 mm from the surface, i.e. considerably deeper than at high concentrations of particles. The maximum temperature drop is 15.2 °C. Near side walls on the side of the entrance part of the cell, temperature is lower by 1.1 °C than at the cell centre.

The decrease of temperature along the cell axis is explained by the absorption of laser radiation during its propagation deep into liquid. The lower temperature near side walls on the side of the front surface of the cell is explained by heat transfer through side walls and from liquid surface; however, heat transfer from the liquid surface at a depth more than 8 mm is virtually absent. Temperature distributions obtained by numerical simulations are in good agreement with experimental results and show that at high concentrations of particles the region of elevated temperature is localised near the surface and low-lying layers are almost not heated. An important result of simulations is the confirmation of the fact that due to the surface heat transfer even in the case of the uniform distribution of nanoparticles in the medium, the maximum heating can be observed not on the layer surface but at some depth. These effects are even more pronounced in the case of the nonuniform distribution of nanoparticles in the volume under study. Temperature fields calculated for this case are presented in Fig. 3. Therefore, the real temperature of deeply lying layers of a biological tissue can be higher than the surface temperature measured with an infrared imager.

3. Experiment

We measured spatial temperature distributions of suspensions of gold particles at different concentrations in eppendorf test tubes and biological tissues *in vivo* for different penetration depths of nanoparticles. The contactless measurements of spatial temperature distributions were performed by using an IRISYS 4010 infrared imager (Infrared Integrated System Ltd., Great Britain). This imager has an uncooled bolometric array, its sensitivity (the temperature difference equivalent to noise) is 0.15 °C, and the range of measured temperatures is $-10 - +250$ °C. The scan rate is eight frames per second, the storage map of the infrared imager provides the recording of up to 6000 thermograms of size 120×120 pixels. The minimal distance from the objective to the object surface providing distinct focusing is 15 cm, and the spatial resolution is no less than 0.3 mm. Thermograms were analysed by using an Imager IRISYS software package.

To perform correct temperature measurements with an IR imager, it is necessary to eliminate the influence of scattered laser radiation. This condition is fulfilled in our case because an IRISYS 4010 infrared imager is sensitive in

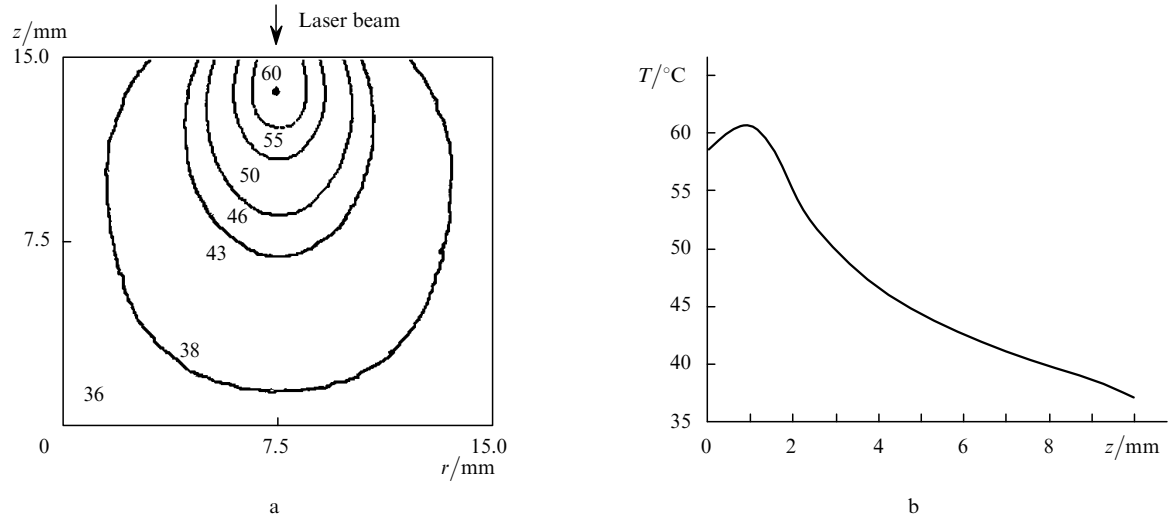

Figure 3. Temperature calculations for a layered system in Fig. 2a exposed to laser radiation: (a) isotherms (figures at the curves indicate temperature in °C; (b) temperature distribution over depth.

the spectral range from 8 to 14 μm, whereas the wavelength of a semiconductor laser used in our experiments was 808 nm.

Figure 4 presents thermograms measured for a colloidal solution of gold nanoshells with a SiO_2 nucleus in a cylindrical cell. The distinct boundaries of the heated region correspond to the cell boundaries. Laser radiation propagated parallel to the cell axis and thermograms were recorded on the side of the cell. Such a configuration allows the temperature distribution over the cell depth to be obtained with a constant error. The independent measurements of temperature with a thermocouple showed that this error did not exceed 2 °C in the temperature range under study. The absence of resonance absorption by the cell walls in the spectral range 6 – 12 μm permits us to compare temperature at the cell centre and on its side surface. Samples were irradiated by a 2-W, 808-nm PhotoThera cw semiconductor laser. The Gaussian beam diameter at the $1/e^2$ level was about 5 mm, which corresponds to an average power density of $\sim$10 W cm^{-2}. At the left and bottom of thermograms are presented the temperature distributions along light straight lines in thermograms (the laser beam direction is shown by the arrow).

The thermal action of laser radiation on biological tissues is based on the absorption of radiation and transformation of its energy to heat. The efficiency of this action depends on its temperature and duration. At temperatures up to 45 °C, no irreversible damage of tissues is expected (cells can be destructed only after prolonged enough heating).

At temperature about 60 °C, the denaturation of proteins occurs rapidly enough. It can be complete or partial, reversible or irreversible. The degree of denaturation depends to a great extent on the action time. The denaturation rates of different protein structures can strongly differ. The critical temperature of the denaturation onset of most of the tissue components under real conditions is about 57 °C.

The noticeable dehydration of biological tissues starts at a temperature of about 70 °C. As the water boiling temperature is achieved, water in tissues transforms to vapour, producing a considerable excess pressure. During slow heating, the vapour has time to escape from a biological tissue through numerous pores, which usually exist or formed under the vapour pressure and also due to thermal destruction of the matrix. This process is called photoevaporation. The heating rate of the tissue at a temperature of about 100 °C considerably decreases due to a considerable consumption of energy for evaporation. After the evaporation of water, the dried tissue is rapidly heated up to a temperature of 150 °C at which the carbonisation process begins. During carbonisation, hydrogen escapes from organic molecules and finely divided carbon (carbon black) is formed.

We present the results of experimental *in vivo* studies of the skin temperature of laboratory animals upon subcutaneous and intramuscular introduction of suspensions of gold nanoparticles. Experiments were performed with white laboratory rats in accordance with standards of humanitarian treatment of animals by the method approved by the committee on ethics at the Saratov State Medical University (protocol n. 13, 10.04.2007). Animals subjected to the general anaesthesia were fixed in the horizontal position on their back and their abdomen was shaved from a diaphragm to a pubic joint before the introduction of nanoparticles. Three sites on each side were marked symmetrically with respect to the middle line of the abdomen. The suspension of gold nanoparticles in amounts of 0.1 mL was introduced by the depth from 0.5 to 5 mm into sites at the right of the middle line. Symmetrical sites at the left of the middle line were used to control temperature produced upon laser irradiation without nanoparticles. The distance from the end of the optical fibre of a laser to the skin surface was 10 mm. The time interval between the introduction of nanoparticles and the beginning of laser action was 2 – 4 min.

The coagulation of the tissue in the site with nanoparticles embedded at a depth of 0.5 mm was observed already within 10 s after continuous laser irradiation. This was visually manifested in the appearance of a white burn spot. After further irradiation, water was evaporated in this spot and the tissue was carbonised. The maximum temperature at the spot centre achieved 180 °C (Fig. 5). The control site without nanoparticles irradiated in the same regime was heated only up to 46 °C. This temperature causes no irreversible damage of the tissue if the heating time does not exceed several minutes.

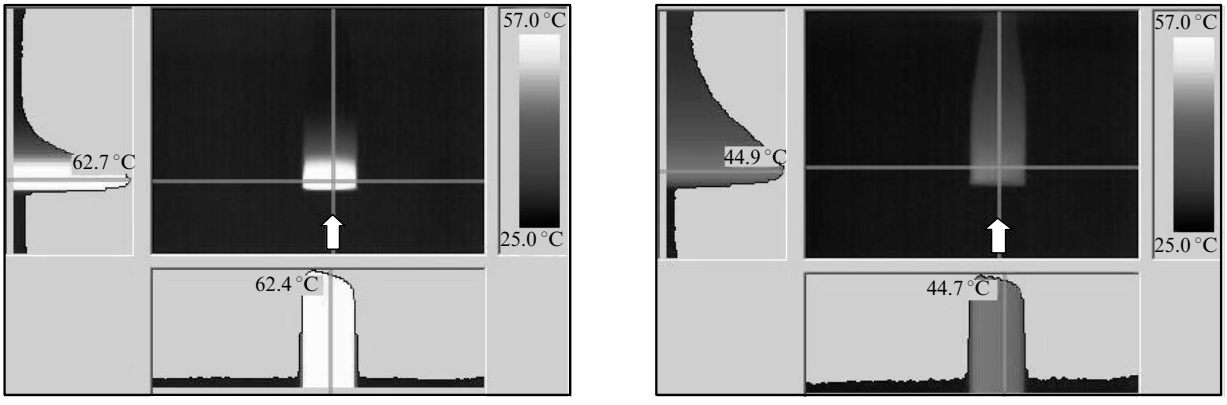

a b

Figure 4. Thermograms of a suspension of plasmon-resonance gold nanoparticles in a 1.5-mL standard eppendorf test tube after irradiation for 2 min by a 2-W cw laser at concentrations of particles 5×10^9 (a) and 0.61×10^9 mL^{-1} (b); the arrow shows the propagation direction of radiation.

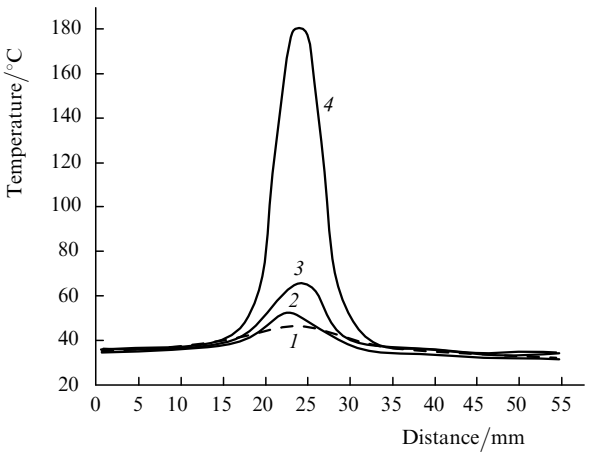

Figure 5. Thermograms of the rat skin *in vivo* obtained directly after laser irradiation for 30 s: (*1*) laser irradiation of a site without nanoparticles; (*2*) intramuscular injection of 0.1 mL of gold nanoshells to a depth of about 5 mm from the skin surface; (*3*) subcutaneous injection (1 mm from the skin surface); (*4*) subcutaneous injection (0.5 mm from the skin surface).

When nanoparticles were embedded at a depth of 5 mm, the maximum temperature at the spot centre after laser irradiation during 30 s achieved 65 °C. This resulted in most cases in visually observed burns, which were confirmed by subsequent histological analyses.

In the case of the intramuscular introduction of nanoparticles to a depth of about 5 mm, no visual changes on the skin of animals was observed after laser irradiation; however, the temperature at the spot centre measured with the infrared imager achieved 52 °C, which is on average exceeds by 6 °C the temperature measured in the control site without nanoparticles irradiated under the same conditions. According to computer simulations, temperature in deep tissue layers for such localisation of the region containing nanoparticles can considerable exceed the surface temperature measured with an infrared imager (Fig. 3b). This experiment is very important for the substantiation of the possibility of hyperthermia of not only surface but also deeper located tumours. The obtained results prove that the photothermolysis of such tumours can be performed without the damage of upper-lying tissues. This conclusion is also confirmed by the results of histological studies.

Independently of the method of introducing nanoparticles and temperature achieved at the centre of a heated region, the size of the region itself where temperature exceeds the temperature of the surrounding tissue (the temperature distribution full width at half-maximum) is virtually the same, amounting to 1 cm. Temperatures obtained in experiments with animals *in vivo* upon local injections of nanoparticles exceed temperatures observed in similar experiments on the laser heating of the colloidal solution of gold nanoparticles in a cell (Fig. 4). This can be explained by the displacement of water from the injection region, whereas nanoparticles remain. A drastic increase in the temperature is observed after the evaporation of water; however, only a very small amount of water is evaporated from a 2-mL cell during irradiation for 2–3 min. Nevertheless, is should be noted that the formation of island structures of coagulated nanoparticles was also observed in some experiments with solutions in cells.

Figure 6 presents the dynamics of the temperature distribution investigated upon continuous and pulsed laser irradiation. Thermograms of the rat skin surface were recorded during heating with intervals of 6 s. The curves in Fig. 6 represent half the symmetric profile of thermograms. The total irradiation time in all cases was 30 s. The irradiation by 2-W, 1-ms laser pulses with an off-duty ratio of 7 was used to obtain temperatures in the range from 40 to 45 °C. This temperature regime is optimal for stimulating apoptosis in tissue cells. In this case, tissue regions not containing nanoparticles are virtually not heated.

4. Conclusions

We have performed computer simulation of the spatial intensity distribution of laser radiation absorbed in samples containing plasmon-resonance particles. Based on the

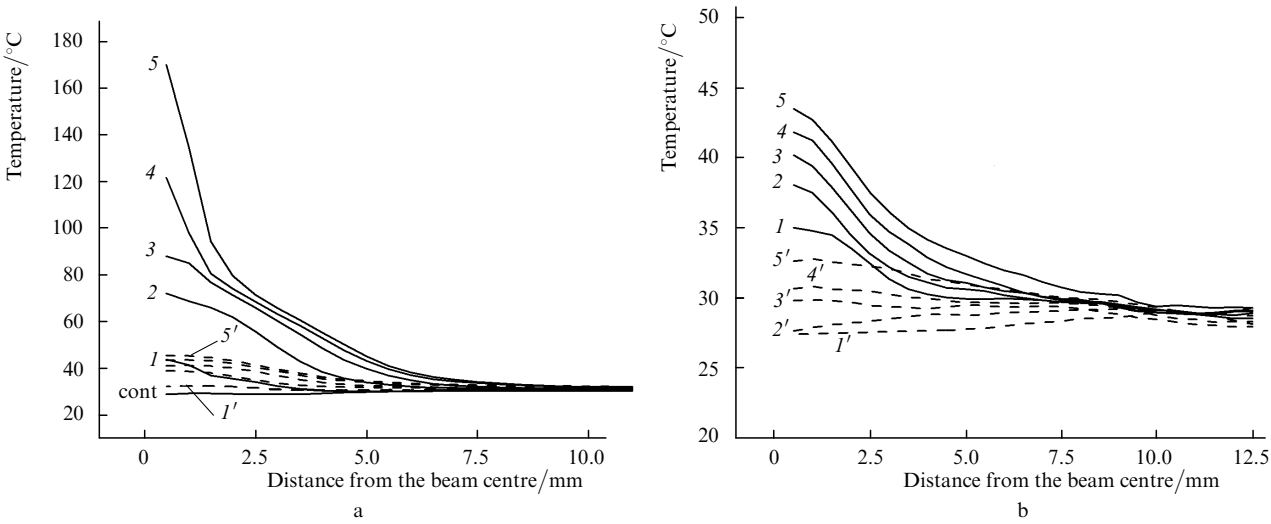

Figure 6. Temperature of the rat skin surface *in vivo* in the region of laser heating upon continuous irradiation by a 2-W laser (a) and upon irradiation by 2-W, 1-ms laser pulses with a off-duty ratio of 7 (b): (*1′–5′*) irradiation in the absence of nanoparticles; (*1–5*) irradiation after the subcutaneous injection of a 0.1-mL suspension of 15-nm-thick nanoshells (with a silicon nucleus of diameter 140 nm) to a depth of 1 mm; (cont) control temperature distribution before heating.

results of simulations, the parameters of thermal sources have been determined in the medium under study and temperature fields produced by these sources have been calculated. Thermal effects appearing upon laser irradiation of colloidal solutions of gold nanoparticles in cells and at different depths of injection of nanoparticles to laboratory animals *in vivo* have been studied experimentally. It has been shown that the temperature of irradiated objects considerably increases in the presence of nanoparticles. The dynamics of laser hyperthermia has been investigated upon continuous and pulsed laser irradiation.

Acknowledgements. This work was supported by the Russian Foundation for Basic Research (Grant Nos 07-02-01434a, 07-04-00301a, 07-04-00302a, and 08-02-00399a). The work of B.N. Khlebtsov was supported by Grants of the President of the Russian Federation (MK 2637.2007.2) and the Foundation for the Support of the Russian Science.

References

1. Yonzon C.R., Zhang X., Zhao J., van Duyne R.P. *Spectroscopy*, **22**, 42 (2007).
2. Kubik T., Bogunia-Kubik K., Sugisaka M. *Cur. Pharmaceutical Biotechnol.*, **22**, 17 (2005).
3. Gobin A.M., Lee M.H., Halas N.J., James W.D., Drezek R.A., West J.L. *Nano Lett.*, DOI: 10.1021/nl070610y (2007).
4. Huang X., Jain P.K., El-Sayed M.A. *Lasers in Medical Science*, DOI: 10.1007/s10103-007-0470-x (2007).
5. Khlebtsov B.N., Zharov V.P., Melnikov A.G., Tuchin V.V., Khlebtsov N.G. *Nanotechnology*, **17**, 5267 (2006).
6. Harris N., Ford M.J., Cortie M.B. *J Phys Chem B*, **110**, 10701 (2006).
7. O'Neal D.P. et al. *Cancer Lett.*, **2009**, 171 (2004).
8. Glomm W.R. *J. Disp. Sci. Tech.*, **26**, 389 (2005).
9. Bogatyrev V.A., Dykman L.A. *Kolloid. Zh.*, **76**, 181 (2007).
10. Khlebtsov N.G., Melnikov A.G., Bogatyrev V.A., Dykman L.A., in *Photopolarimetry in Remote Sensing. NATO Science Series, II. Mathematics, Physics, and Chemistry*. Ed. by G. Videen, Ya.S. Yatskiv, M.I. Mishchenko (Dordrecht: Kluwer, 2004) Vol. 161, pp 265 – 308.
11. Paciotti G.F., Myer L., Weinreich D., Goia D., Pavel N., McLaughlin R.E., Tamarkin L. *Drug. Delivery*, **11**, 169 (2004).
12. Hirsch L.R., Gobin A.M., Lowery A.R., Tam F., Drezek R.A., Halas N.J., West J.L. *Ann. Biomed. Eng.*, **34**, 15 (2006).
13. Kalele S., Gosavi S.W., Urban J., Kulkarni S.K. *Cur. Nanoscience*, **91**, 1038 (2006).
14. Irani G.B., Huen T., Wooten F. *J. Opt. Soc. Am.*, **61**, 128 (1971).
15. Otter M.Z. *Physik*, **161**, 163 (1961).
16. Johnson P.B., Christy R.W. *Phys. Rev. B*, **12**, 4370 (1973).
17. Izotova V.F., Maksiova I.L., Romanov S.V. *Opt. Spektrosk.*, **89**, 86 (2000).
18. Rozenfel'd L.G., Kolotilov N.N. *Onkologiya*, **3**, 103 (2001).
19. Maksimova I.L., Akchurin G.G., Khlebtsov B.N., Terentyuk G.S., Akchurin G.G., Ermolaev I.A., Skaptsov A.A., Soboleva E.P., Khlebtsov N.G., Tuchin V.V. *Med. Laser Applications*, **22**, 199 (2007).
20. Zenkevich O.C., Morgan K. *Finite Elements and Approximation* (New York: John Willey & Sons, 1983; Moscow: Mir, 1986).